Оптический журнал

Лазерная физика и техника

Generation of high-quality non-diffracting beams using spatial filtering

© 2020 Ying Zhang*, **, doctoral student; Ke Fan***, PhD; Jianzhong Lou***, MS; Yan Wei*, **, PhD

*Institute of Optics and Electronics, Chinese Academy of Sciences, Chengdu, 610209, China;
**University of Chinese Academy of Sciences, Beijing, 100049, China;
***Guangzhou Institutes of Biomedicine and Health, Chinese Academy of Sciences, Guangzhou, 510530, China

E-mail: fan_ke@gibh.ac.cn, yanwei@ioe.ac.cn

Submitted 24.12.2019

DOI:10.17586/1023-5086-2020-87-06-09-17

Annular spatial filtering is a widely used technique for the generation of non-diffracting beams. Combined with a phase modulator, this setup can generate arbitrary non-diffracting beams with high power efficiency. Previously, researchers have mainly focused on the generation of a specific type of beam (Bessel, Weber). In this study, a method to obtain the optimal setup parameters for general non-diffracting beams was introduced. To achieve the balance of efficiency and beam quality, appropriate sampling numbers and annular ring size were determined. A simulation, derived from the Fourier optics model, was developed to estimate the optimal parameters. The selected ring width predicted by the simulation was then verified using experimental results. This investigation develops a strategy to improve the quality of various non-diffracting beams in more general applications.

Keywords: *non-diffracting beams, high-quality, spatial filtering.*

OCIS codes: *260.0260.*

Генерация высококачественных недифрагирующих пучков с использованием пространственной фильтрации

© 2020 г. Ying Zhang, Ke Fan, Jianzhong Lou, Yan Wei

Для генерации недифрагирующих пучков широко применяется кольцевая пространственная фильтрация. В сочетании с фазовым модулятором это позволяет генерировать произвольные типы недифрагирующих пучков с высокой энергетической эффективностью. Ранее исследователи в основном фокусировали свое внимание на генерации специфических типов пучков (Бесселя, Вебера). В настоящее работе предложен метод получения оптимальных параметров фильтрации для получения недифрагирующих пучков общего вида. Развита теория и проведено численное моделирование процесса фильтрации, основанное на использовании методов фурье-оптики. Определены параметры выборочной совокупности и размеры диафрагмирующего кольца, обеспечивающие баланс эффективности преобразования и качества пучков. Определенные таким образом параметры были верифицированы с использованием экспериментальных результатов. Выполненные исследования позволяют сформировать стратегию улучшения качества недифрагирующих пучков общего вида применительно к конкретным приложениям.

Ключевые слова: *недифрагирующие пучки, высокое качество, пространственная фильтрация.*

1. INTRODUCTION

Non-diffracting beams (NBs) were first demonstrated by Durnin [1] as a set of solutions to the Helmholtz equation. Theoretically, they have a diffraction-free property during propagation. NBs have been investigated in various optical applications, such as nonlinear optics [2], optical trapping [3], and holographic lithography [4]. Group theory showed that NBs can be separated into four different categories [5]: discrete non-diffracting beams (DNB) [6], Bessel beams [7], Mathieu beams [8], and parabolic beams [9]. The distinction between these categories is based on the expression of NBs in the Cartesian, circular cylindrical, elliptical cylindrical, and parabolic cylindrical coordinates. Theoretically, the electromagnetic field of NBs requires infinite energy to have an arbitrary diffraction free distance. However, a good approximation of NBs could be implemented in practice, under a finite distance and energy [10]. The generation of approximate NBs can be done using two methods: one can construct the NB's angular spectrum characteristic in Fourier Optics, or directly modulate it on a plane wave. The first experimental generation of a J_0 Bessel field utilized an annular slit in the front focal plane of a positive lens, illuminated by the plane wave [11]. By replacing the annular slit with a digital micromirror device (DMD) [12], the beam spot sizes of the Bessel beams could be modified. An additional scattering diffuser produced a random NB before the annular slit [13]. Spatial light modulators (SLM) provide another choice for further modulation [14]. However, the beam loss through the annular slit aperture results in very low energy transmission for this type of method. Currently, direct modulation still experiences technological constraints, because efficient phase and amplitude modulation are difficult to achieve simultaneously. The use of a filter with the complex-amplitude transmittance of Bessel beams was introduced by Durnin [15]. A more flexible method is to modulate a plane wave using binary amplitude-phase hologram [16]. However, the most common method is to use a refractive element with a conical surface, known as an axicon [17], which can produce a ring after the Fourier transforms, to form an approximation of the J_0 Bessel field [7, 18]. It was also reported that by using different illumination strategies, higher-order Bessel fields can still be produced with an axicon [19]. Diffractive axicons are widely used for their flexibility in terms of the selection of optical elements, such as SLMs [20–22], waveguides [23], DMDs [24], and segmented deformable mirrors [25]. With a diffractive axicon, the random generation efficiency is significantly increased for any random NB patterns [26]. When using an axicon, further modulation is typically in the Fourier domain adjacent to the annular ring. However, the precision of modulation is very restricted due to the conflict between the thin width of the ring and the resolution of the optical elements. An alternative solution is to modulate the phase of the desired field with the annular slit. Other studies have shown that this setup can efficiently generate arbitrary limited distance NBs [27, 28]. However, a difference in the width of the annular ring will influence the quality and energy transmittance of the beam [29].

In this paper, we further investigated the influence of the ring shape and parameter choice for arbitrary NBs. Furthermore, a simulation model based on Fourier optics, was developed to optimize the parameter selection. Finally, a phase-only SLM and annular rings of different sizes were used to build an optical setup for experimental and verification purposes. The experimental measurements were compared to the theory to verify the analysis.

2. THEORETICAL ANALYSIS

NBs have the distinctive feature of an invariant transverse profile during propagation. The light field of NBs can be expressed as $E(r, z) = \varphi(r)\exp(\mathrm{i}k_z z)$, where the transverse field is independent of the propagation direction z.

In the Whittaker integral form, the light field of non-diffracting beams can be defined using circular cylindrical coordinates

$$E(r,\theta,z) = \\ = \exp(\mathrm{i}\,k_z z)\int_0^{2\pi} A(\phi)\exp(\mathrm{i}\,k_t r\cos(\phi-\theta))d(\phi). \quad (1)$$

Here, k_z and k_t are the longitudinal and transverse components of wave numbers, respectively, which can be expressed as $k^2 = k_z^2 + k_t^2$.

r and θ are the radial and azimuthal spatial transverse coordinates, respectively. $A(\phi)$ is the angular spectrum function and can be discretized with Dirac delta function as

$$A(\phi) = \sum_{n=1}^{N} a_n \exp(ib_n)\delta(\phi - \phi_n), \quad (2)$$

where a_n and b_n are the amplitude and phase parameters of plane waves in the frequency domain, respectively. A light field can be comprehended as an interference field of those plane waves. δ is the Dirac delta function, $\phi_n = 2\pi n/N$. N is the number of plane waves, also called the sampling number. Substituting Eq. (2) into Eq. (1)

$$E(r,\theta) = \sum_{n=1}^{N} a_n \exp(ib_n)\exp[ik_t r\cos(\phi_n - \theta)], \quad (3)$$

which is a linear combination of plane waves with arbitrary coefficients. All NBs can be generated by different a_n, b_n, N and k_t, including the four fundamental categories outlined in Eq. (3). The k_t in Eq. (3) determines the transverse scale of an NB. The choice of N is dependent on the reconstruction requirement of the sampling number for $A(\phi)$, and a_n, b_n determine the chosen $A(\phi)$ function. For example, a simple DNB can be considered as an interference of the light fields of plane waves, set with $a_n = 1$, $b_n = 1$ and varying N.

In this paper, the beam generation setup used a phase-only modulator associated with an annular slit, which is shown in Fig. 1a. The accurate phase of the chosen NB was applied to the SLM. Between the two lenses, the annular slit was used as a bandpass filter. The charge-coupled device (CCD) camera was placed in the focal plane to capture the NB transverse profile. A Fourier optics approach was applied for the numerical calculations. The simulation assumed that the initial light field profile was a collimated beam. It was first modulated by the SLM, which multiplied the phase of the given NB profile. A Fourier transform was used to simulate the focal plane after lens L1. The annular ring mask was considered an aperture, and only allowed light to pass through the ring slit, which can be seen as a binary bandpass filter. The output beam, after lens L2, could be achieved using an inverse Fourier transform. The generated NBs could be obtained after the inverse Fourier transform function was applied to the filtered beam.

Therefore, the light field on the SLM could be defined as $E_0 = E(r, \theta)/|E(r, \theta)|$, which is the phase-only modulation on a uniformly illuminated beam. The field on the focal plane of lens L1 is the Fourier transform of $E_0(r, \theta)$, which can be evaluated as:

$$E_1(r,\theta) = \lambda f_1 S(\rho,\phi) = \lambda f_1 \mathcal{F}[E_0(r,\theta)], \quad (4)$$

where $\mathcal{F}$ denotes the Fourier transform operation, ρ and ϕ are spatial frequencies in polar coordinates, respectively, f_1 is the focal length of lens L1, and λ is the wave length of the laser beam. If the ring mask is considered as a "no edge diffraction"

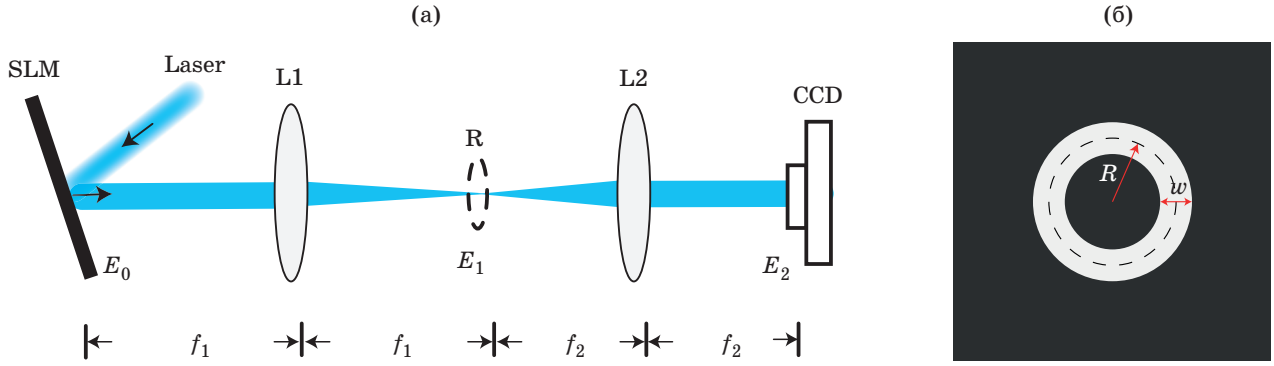

Fig. 1. Core parts of the optical system. (a) Schematic of a 4-f spatial filtering optical system used to generate NBs. This system includes a collimating laser source (405 nm), an SLM, an input lens of filter stage (L1 with focal distance f_1), a ring mask (R) set on the Fourier plane of L1, and a CCD, which is a camera placed at the output of the 4f system. (b) Schematic of the circular mask at the entrance of the 4f system. The shadow section of the image represents the area where the light is blocked.

filter, it can be expressed as a spatial filtering function

$$H(r)=\begin{cases}1 & |r-R|\le\dfrac{W}{2}\\ 0 & |r-R|>\dfrac{W}{2}\end{cases}, \tag{5}$$

where R and W represent the radius and the width of the ring slit, respectively (Fig. 1b). At the detection plane of the CCD, the output light field can be written as

$$I_{\text{image}}(r,\theta)=\left|E_2(r,\theta)\right|^2=$$
$$=\left|\frac{f_2}{f_1}\mathcal{F}^{-1}[\mathrm{H}(r)E_1(r,\theta)]\right|^2, \tag{6}$$

where $E_2(r, \theta)$ is the light field on the focal length of L2, $\mathcal{F}^{-1}$ denotes the inverse Fourier transform, and f_2 is the focal length of lens L2.

3. SIMULATIONS AND EXPERIMENTS

3.1. Upper boundary of sampling number *N*

The diversity of NBs is dependent on the angular spectrum function $A(\phi)$ in Eq. (2). The finiteness, resolution, and size of the SLM limited the representation capability of the whole system. This led to an upper boundary $N_{\max}$ of the sampling number N in Eq. (2). From a Fourier optics point of view, it is possible to approximate a reasonable $N_{\max}$. The time-spatial transformation denotes the relationship between the frequency resolution Δp_f and the sampling rate of the SLM f_s.

$$\Delta f=\frac{f_s}{M}=\frac{1}{\Delta pM}. \tag{7}$$

Here, the sampling rate can be calculated based on the SLM's pixel size, which is $f_s = 1/\Delta p$. M is the pixel number of the light field, which is also dependent of the SLM. According to the transformation between the coordinates on the focal plane of L1 and the frequency domain of the light field, the resolution Δp_f at the focal plane of L1 can be expressed as follows:

$$\Delta p_f=\lambda f_1\Delta f. \tag{8}$$

However, the radius of the focused ring at L1 can be expressed as:

$$R=\frac{\lambda}{\lambda_t}f_1, \tag{9}$$

where the transverse components of wavelength $\lambda_t = 2\pi/k_t$. Therefore, the theoretical $N_{\max}$ is equal to the sampling size on the entire ring, which is

$$N_{\max}=\frac{2\pi R}{\Delta p_f}=\Delta pMk_t. \tag{10}$$

It is important to note that $N_{\max}$ is only related to the size of the SLM and the chosen k_t. A larger SLM size can provide a higher sampling rate on the angular spectrum function $A(\phi)$.

3.2. The choice of ring mask parameters

The radius and width of the Durning ring are additional essential factors which influence the generation quality of this setup. A structural similarity (SSIM) index, which is a method for image quality evaluation, was applied to quantify the effects of different parameters. SSIM index is a perceptual metric that quantifies image quality, which is based on visible structures in the image [30]. Before computing the SSIM, all light intensity was normalized to the [0, 1] range for comparison. For the general case where the input of the SLM is uniformly illuminated, the simulation was performed using the fast Fourier transform algorithm. The SLM parameters were set with a 600×600 pixels number and 20×20 μm pixel size to meet the practical needs. The focal length of L1 was 0.5 m and the wavelength λ of the light was 405 nm.

The four categories of NBs in four different λ_t setups were respectively tested to estimate the relation between ring width and NB quality (shown in Fig. 2). Each type had 20 subjects, which resulted in a 0–20 order Bessel beam, 0–20 order Mathieu beam with a random ellipticity parameter, 20 Weber beams with a random parameter, and 20 DNBs with different N. Additionally, 50 NBs with random a and b were used to test the general case. In the simulation results, the different types of beams behaved differently when the width of ring changed. However, all types reached an optimal width of approximately 0.040 mm. The scale was similar to the size of an Airy disk, which was

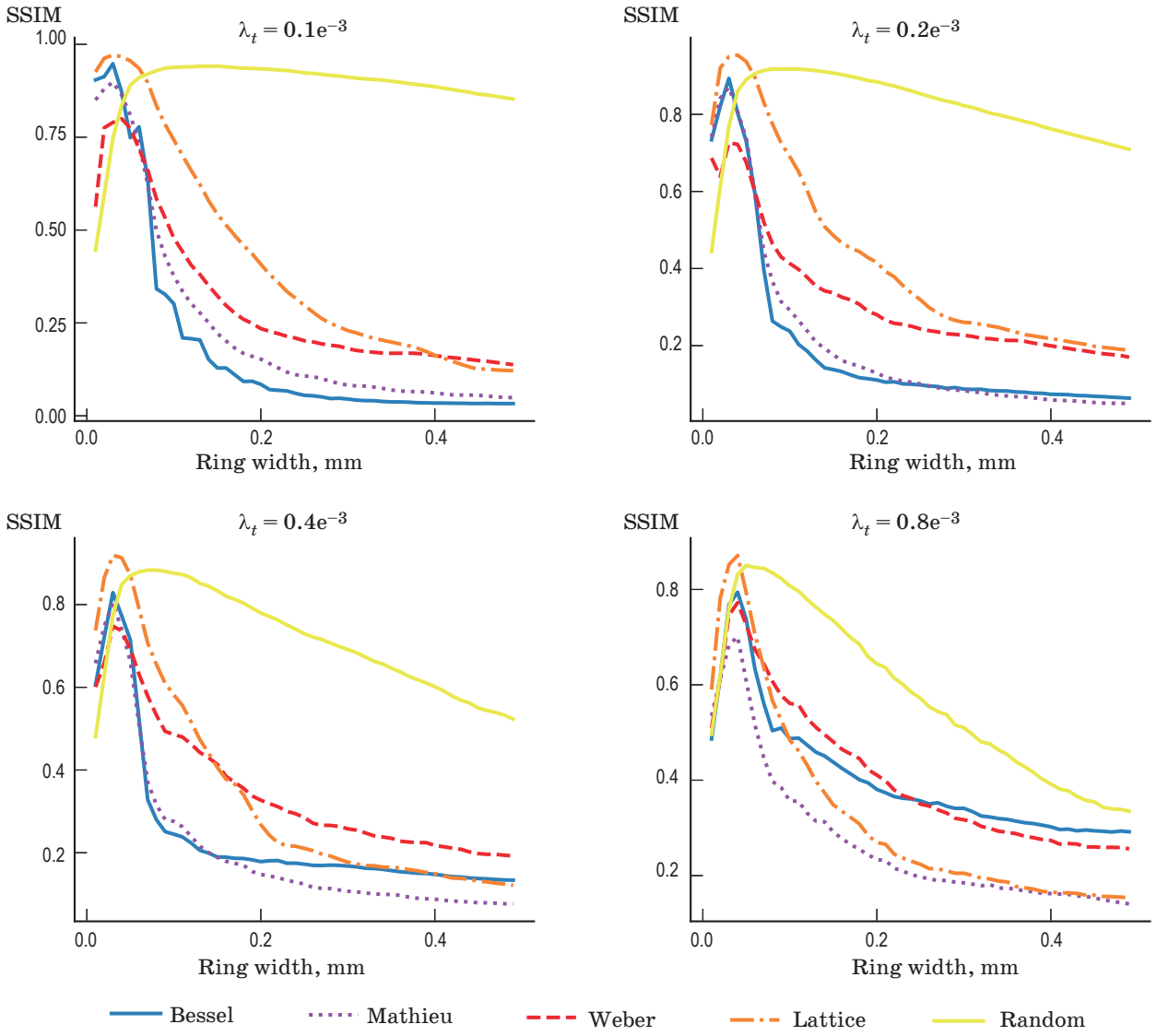

Fig. 2. SSIM index on generated NBs for different ring widths.

0.042 mm in this setup. To further investigate a general optimal width for arbitrary NBs, the mean and standard deviation of all similarity were plotted in Fig. 3. The optimal ring width to be adopted was in the range of 0.030–0.050 mm, from the most similarity and smallest diversity. Considering the influence of noise, the radius had no significant effect on the ring width selection.

Compared to Durnin's technique, one advantage of the 4-f optical system is the effective utilization of laser power. This will be beneficial to many optical applications, such as, optical trapping, holographic lithography, etc. The influence of different ring widths on the optical power are presented in Fig. 4. The utilization is

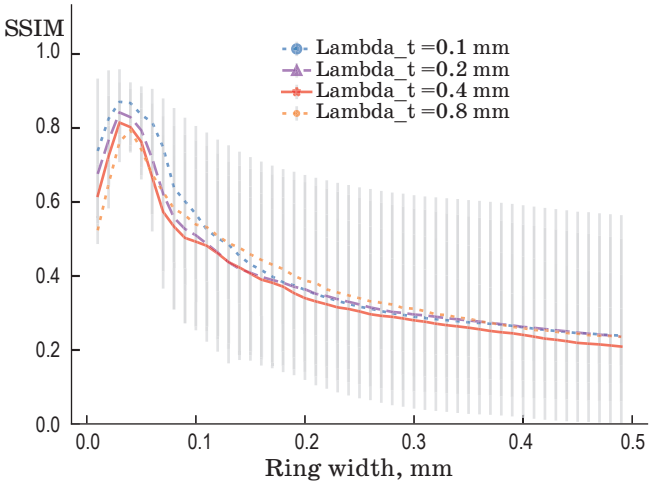

Fig. 3. SSIM index on different λ_t of NBs for different ring widths.

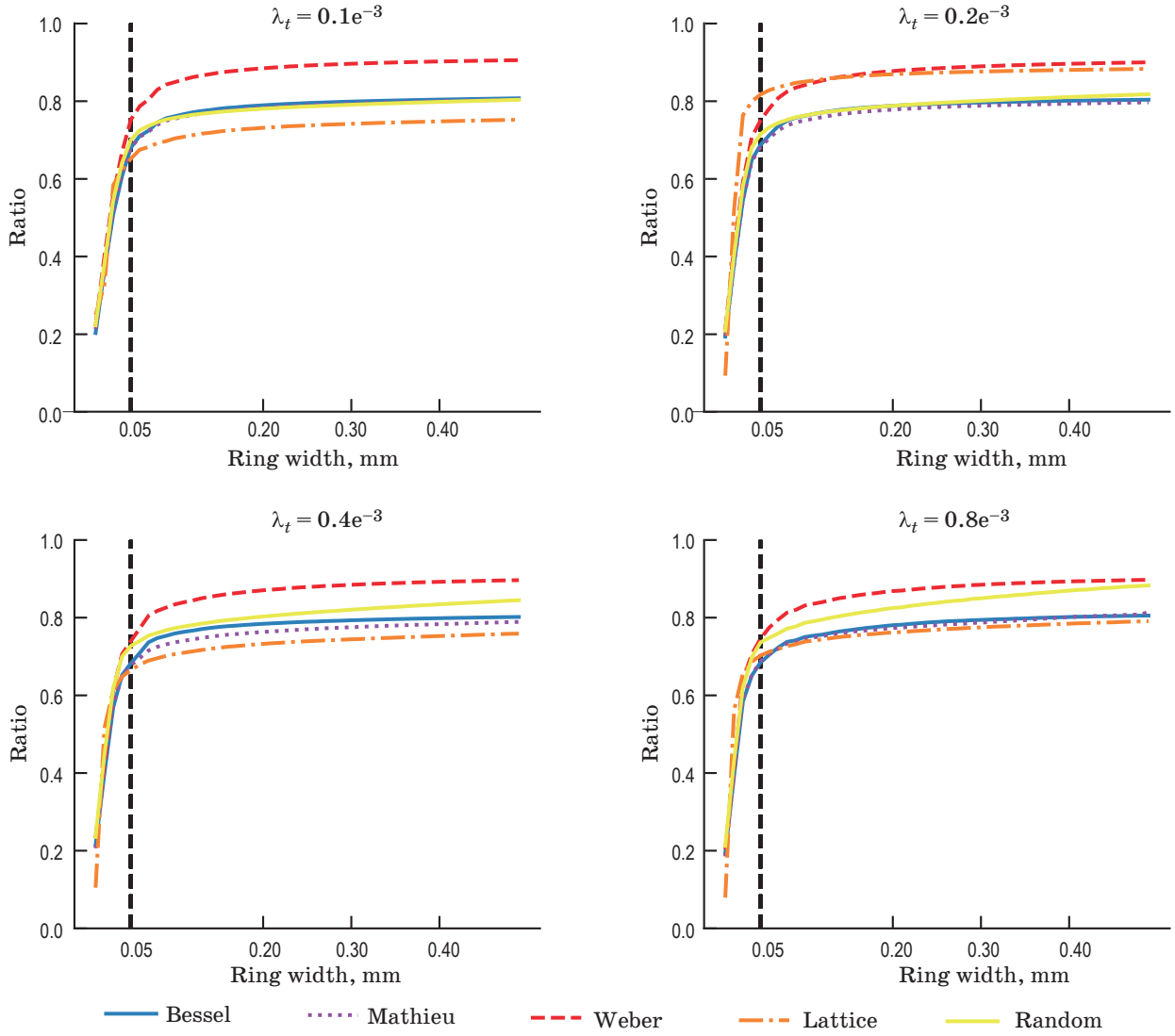

Fig. 4. The average value of the remaining power ratio of the NBs for different ring widths.

defined as the ratio between the output power $|E_2|^2$ and input power $|E_0|^2$.

In Fig. 4, the average value of the remaining power ratio of NBs is displayed for different ring widths. The utilization had a slight difference for different NB types. However, when the width reached 0.050 mm in the optimal range, the efficiency became steadily larger than 60%. While the width of the ring reached 0.1 mm, the curve became flatter, and the remaining power ratio of the NBs was more than 60%.

3.3. Optical experiments

For the verification of the above simulation of the ring width optimization, two differently sized rings were applied. The experimental setup is shown in Fig. 5. Light from a He-Ne laser

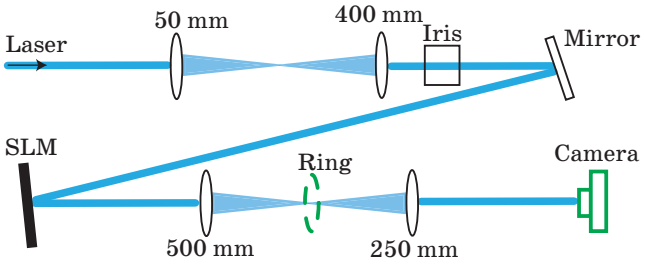

Fig. 5. Schematic of the experimental light pathway.

source (500 mW, 405 nm) was reduced through neutral-density filters (Thorlabs) and collimated by lenses ($f = 50$ mm and $f = 400$ mm) and irises (Edmund 35110). A phase-only SLM (HAMAMATSU, LCOS-SLM X10468-01, reflective) was illuminated by the collimated light. The SLM

pixel size was 20×20 μm^2 and the resolution was 800×600 pixels. A positive lens L1 ($f_1 = 500$ mm) was placed after the SLM to obtain a frequency light field. Customized radius of 0.925 mm was selected, with two different widths (50 μm and 150 μm). The output profile was monitored by a CCD camera (PCO, Pixelfly USB, 1392×1040 pixels) after lens L2 ($f_2 = 250$ mm).

In the experiments, we demonstrated three examples of typical generated NBs, which were zero-order Bessel beams, 10-order even Mathieu beams, and even Weber beams. For the zero-order Bessel beam, the coefficients a_n and b_n were set to 1 and 0, respectively. For the Mathieu beam, the order $m = 10$ and the ellipticity parameter $q = 30$, in the angular spectrum formula

$$A(\phi) = ce_m(\phi, q). \tag{11}$$

The Weber beam used the angular spectrum formula

$$A(\phi) = \frac{1}{2\sqrt{\pi|\sin(\phi)|}} \exp\left(ia \ln\left|\tan\frac{\phi}{2}\right|\right), \tag{12}$$

where $a = -2$. For both types, N was set to $N_{\max} = 377$, to maximize the representation capability.

All captured images were normalized, based on the maximum intensity. The experimental results are displayed in Fig. 6. The simulation and experimental measurements were nearly identical at the center, however, there is a noticeable intensity difference near the image edge. This intensity variation may be caused by the light source in the experimental setup, which was not an ideal plane wave. All numerical and experimental results confirmed that the image qualities were higher at a 50 μm ring width, regardless of the NB type. This observation is subject to the simulation analysis of the ring width choice. As the ring width increased, the intensity of the side lobe increased, which influenced the image's similarity to the ideal NBs.

Quantitative measurements on the SSIM (shown in Fig. 7) verified the observation that the image quality decreased when the ring width selection was out of the optimal range

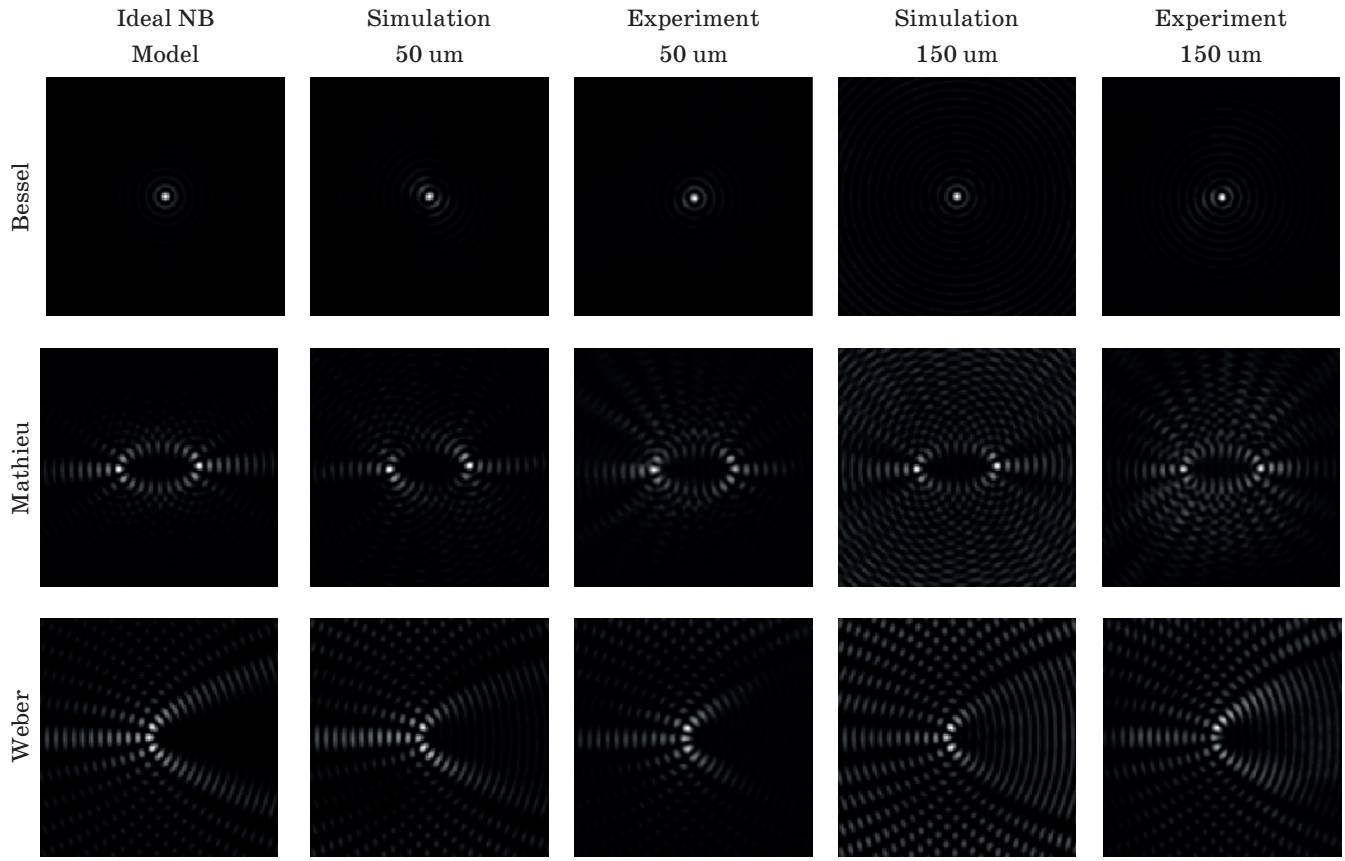

Fig. 6. Simulated and experimental images of Bessel, Mathieu, and Weber beams. The size of the patterns detected by the CCD was 1.5 mm.

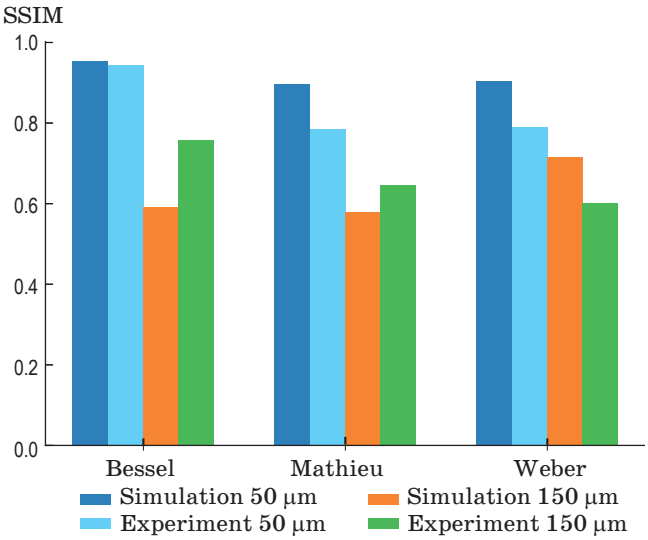

Fig. 7. SSIM index of the simulated and experimental results for different ring widths.

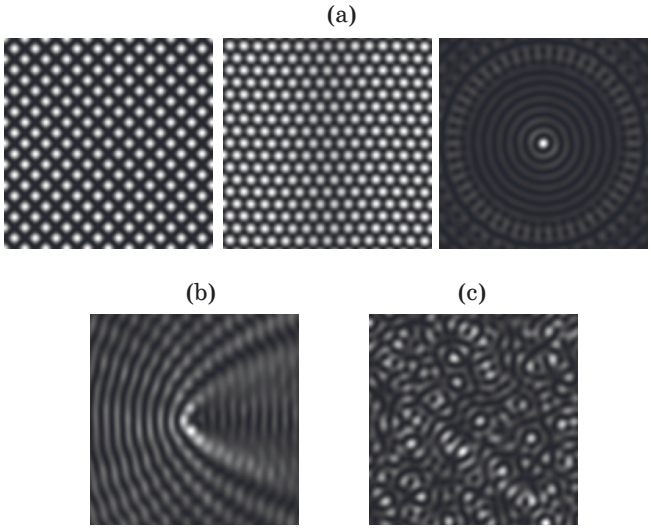

Fig. 8. Simulated examples for real applications. (a) Multi-beam interference pattern, (b) continuous Weber beam pattern, and (c) random NB pattern.

in the simulation. Based on the simulated image size, the photographs taken by the camera were resized using bilinear interpolation in the OpenCV package. We have observed that the experimental results sometimes vary in terms of quality and similarity. This is most likely due to the pixelization of the ring mask, which may introduce an error to the smooth real scenario. However, this did not influence the strategy for the selection of the parameters.

The optimized optical system can produce various high-quality high-power NBs, which are directly implemented in optical applications. For example, the setup can generate multi-beam interference patterns for lithography [4], which are shown in Fig. 8a. The continuous Weber beam pattern can be designed to manipulate micro-particles, similar to a previous study [31], as shown in Fig. 8b. Moreover, the setup easily produces random NB patterns [26], which may attract considerable research interest in the field of information encryption (Fig. 8c).

4. CONCLUSION

In order to achieve a balance between flexibility and efficiency in the generation of arbitrary NBs, we have built an optical setup using a Durnin ring with a phase-only SLM. A model of the angular spectrum function was built to estimate the upper boundary of the sampling rate. A simulation method, based on Fourier optics, was developed to study the relationship between the beam quality and parameters. This relationship was measured using an image similarity SSIM. All the numerical calculations were verified using an experiment optical setup. The experiments proved that the optimal ring width range can be effectively estimated by the simulation method. We believe that this method of optimal parameter suggestion can assist with the implementation of non-diffracting beams in general applications.

This work was supported in part by The Instrument Developing Project of the Chinese Academy of Sciences, Grant No.YA17K014 and NO.Y74H011.

REFERENCES

1. *Durnin J.* Exact solutions for nondiffracting beams. I. The scalar theory // Journal of The Optical Society of America A-optics Image Science and Vision. 1987. V. 4. No 4. P. 651–654.
2. *Fleischer J.W., Segev M., Efremidis N.K., Christodoulides D.N.* Observation of two-dimensional discrete solitons in optically induced nonlinear photonic lattices // Nature. 2003. V. 422. No 6928. P. 147–150.
3. *Garceschavez V., Mcgloin D., Melville H., Sibbett W., Dholakia K.* Simultaneous micromanipulation in multiple planes using a self-reconstructing light beam // Nature. 2002. V. 419. No 6903. P. 145–147.

4. *Zhou Q., Yang W., He F., Stoian R., Hui R., Cheng G.* Femtosecond multi-beam interference lithography based on dynamic wavefront engineering // Optics Express. 2013. V. 21. No 8. P. 9851–9861.
5. *Bouchal Z.* Nondiffracting optical beams: physical properties, experiments, and applications // Czechoslovak Journal of Physics. 2003. V. 53. No 7. P. 537–578.
6. *Boguslawski M., Rose P., Denz C.* Increasing the structural variety of discrete nondiffracting wave fields // Physical Review A. 2011. V. 84. No 1. P. 013832.
7. *Scott G., Mcardle N.* Efficient generation of nearly diffraction-free beams using an axicon // Optical Engineering. 1992. V. 31. No 12. P. 2640–2643.
8. *Alpmann C., Bowman R., Woerdemann M., Padgett M.J., Denz C.* Mathieu beams as versatile light moulds for 3D micro particle assemblies // Optics Express. 2010. V. 18. No 25. P. 26084–26091.
9. *Bandres M.A., Gutierrezvega J.C., Chavezcerda S.* Parabolic nondiffracting optical wave fields // Optics Letters. 2004. V. 29. No 1. P. 44–46.
10. *Overfelt P.L., Kenney C.S.* Comparison of the propagation characteristics of Bessel, Bessel–Gauss, and Gaussian beams diffracted by a circular aperture // Journal of The Optical Society of America A-optics Image Science and Vision. 1991. V. 8. No 5. P. 732–745.
11. *Durnin J., Miceli J.J., Eberly J.H.* Diffraction-free beams // Physical Review Letters. 1987. V. 58. No 15. P. 1499–1501.
12. *Wang Y., Qu W., Jiao L., Zhang Y.* Generation and control of Bessel beams based on annular reflections // Applied Physics B. 2015. V. 119. No 2. P. 241–245.
13. *Turunen J., Vasara A., Friberg A.T.* Propagation invariance and self-imaging in variable-coherence optics // Journal of The Optical Society of America A-optics Image Science and Vision. 1991. V. 8. No 2. P. 282–289.
14. *Vasilyeu R., Dudley A., Khilo N.A., Forbes A.* Generating superpositions of higher order Bessel beams // Optics Express. 2009. V. 17. No 26. P. 23389–23395.
15. *James D., Joseph E.* Diffraction free arrangement // United States Patent No. 4887885. 1989.
16. *Vasara A., Turunen J., Friberg A.T.* Realization of general nondiffracting beams with computer-generated holograms // Journal of The Optical Society of America A-optics Image Science and Vision. 1989. V. 6. No 11. P. 1748–1754.
17. *Mcleod J.H.* The axicon: a new type of optical element // Journal of the Optical Society of America. 1954. V. 44. No 8. P. 592–597.
18. *Indebetouw G.* Nondiffracting optical fields: some remarks on their analysis and synthesis // Journal of The Optical Society of America A-optics Image Science and Vision. 1989. V. 6. No 1. P. 150–152.
19. *Arlt J., Dholakia K.* Generation of high-order Bessel beams by use of an axicon // Optics Communications. 2000. V. 177. No 1. P. 297–301.
20. *Davis J.A., Carcole E., Cottrell D.M.* Nondiffracting interference patterns generated with programmable spatial light modulators // Applied Optics. 1996. V. 35. No 4. P. 599–602.
21. *Chattrapiban N., Rogers E.A., Cofield D., Hill W.T., Roy R.* Generation of nondiffracting Bessel beams by use of a spatial light modulator // Optics Letters. 2003. V. 28. No 22. P. 2183–2185.
22. *Bowman R., Muller N., Zambranapuyalto X., Jedrkiewicz O., Trapani P.D., Padgett M.J.* Efficient generation of Bessel beam arrays by means of an SLM // European Physical Journal – special Topics. 2011. V. 199. No 1. P. 159–166.
23. *Shen T., Lang T., Wu M., Han Z.* Bessel-like beam generated by an axicon based on parallel-plate waveguides // Applied Optics. 2018. V. 57. No 21. P. 6174–6180.
24. *Gong L., Ren Y., Xue G., Wang Q., Zhou J., Zhong M., Wang Z., Li Y.* Generation of nondiffracting Bessel beam using digital micromirror device // Applied Optics. 2013. V. 52. No 19. P. 4566–4575.
25. *Yu X., Todi A., Tang H.* Bessel beam generation using a segmented deformable mirror // Applied Optics. 2018. V. 57. No 16. P. 4677–4682.
26. *Cottrell D.M., Craven J.M., Davis J.A.* Nondiffracting random intensity patterns // Optics Letters. 2007. V. 32. No 3. P. 298–300.
27. *Hernandezhernandez R.J., Terborg R.A., Ricardezvargas I., Volkesepulveda K.* Experimental generation of Mathieu–Gauss beams with a phase-only spatial light modulator // Applied Optics. 2010. V. 49. No 36. P. 6903–6909.
28. *Arrizon V., Sanchezdelallave D., Ruiz U., Mendez G.* Efficient generation of an arbitrary nondiffracting Bessel beam employing its phase modulation // Optics Letters. 2009. V. 34. No 9. P. 1456–1458.
29. *Mahmoud M., Shalaby M., Khalil D.* Propagation of Bessel beams generated using finite-width Durnin ring // Applied Optics. 2013. V. 52. No 2. P. 256–263.
30. *Wang Z., Bovik A.C., Sheikh H.R., Simoncelli E.P.* Image quality assessment: from error visibility to structural similarity // IEEE Trans Image Process. 2004. V. 13. No 4. P. 600–612.
31. *Liu W., Gao J., Yang X.* Optical transportation of micro-particles by non-diffracting Weber beams // Journal of Optics. 2018. V. 20. No 12. P. 125401.